Dynamic Article Links ▶

PAPER

Mixed-metal substrates for applications in metal-enhanced fluorescence†

Karina Golberg,[a] **Amit Elbaz,**[a] **Yongxia Zhang,**[b] **Anatoliy I. Dragan,**[b] **Robert Marks**[a] **and Chris D. Geddes**[*b]

Over the last decade Metal-Enhanced Fluorescence (MEF) has emerged as the next generation of fluorescence spectroscopy, *i.e.* near-field fluorescence. However, in contrast to our collective knowledge and understanding of classical far-field fluorescence, we know relatively little. MEF is a consequence of the near-field interactions of fluorophores (dipoles) with the surface plasmons generated in plasmon supporting materials, where the optical properties of the metal afford for a wavelength dependence of MEF. In this paper we show that we are not limited to the properties of the individual metals for MEF, but in fact, surface deposits of *mixed metals* can create new dephased plasmon resonance bands, not present in the individual metals themselves. Subsequently, mixed metal substrates (MMS) offer significant opportunities for the multifarious and forever growing applications of MEF.

1.0 Introduction

In the last decade the interaction of fluorophores with metallic nano-particles has attracted significant literature,[1–5] with numerous applications focused at the life sciences.[2,6–9] Fluorophore near-field interactions with plasmon supporting materials typically lead to enhanced fluorescence signatures,[3,5,10,11] and reduced fluorophore lifetimes, which, invariably lends itself to enhanced fluorophore photostabilities. Enhanced chemiluminescence signatures[12] as well as enhanced triplet yields have also been reported from different metallic surfaces,[13] with enhanced triplet yields giving rise to a variety of favorable Reactive Oxygen Photophysics, such as enhanced singlet oxygen and superoxide anion radical generation.[14,15] The wavelength dependence of MEF has also recently been postulated,[16] as well as the angular dependence of emission,[17] the distance dependence of MEF,[18] as well as excitation volumetric effects (EVE), which readily allows for tunable luminescence enhancement factors. Since MEF was defined nearly a decade ago[3] and the mechanism postulated only a few years later,[19] nearly all the reports of MEF have involved the exclusive use of single metallic substrates. Several reports of mixed metal *continuous film coatings* for SPCF and particularly substrates utilizing dielectric coatings or spacer layers *e.g.* SiO$_2$ and SiO$_x$ can be found in the research literature.[20,21] There is also a significant literature on the plasmonics properties of metal–metal coatings; we note the excellent works of Halas *et al.*,[22,23] although none of these reports involve near-field dipoles and enhanced fluorescence signatures.

In this manuscript we subsequently show that mixed-metal coatings of both silver and aluminium nanoparticles readily afford for enhanced luminescence intensities, more so than the individual metals alone. In addition, the presence of two metals creates a new dephased plasmon resonance band, not evident in the optical properties of each individual metal. Our findings suggest that mixed metal substrates may well be an approach for developing surfaces for broad wavelength enhancement and to some degree overcoming the single-metal wavelength dependence of MEF.[16] In this manuscript, we subsequently show that MMS are ideal for enhancing the luminescence of intrinsic protein residues such as phenylalanine and tryptophan, as well as visible wavelength fluorophores such as fluorescein. In addition, a much more pronounced photostability is observed for fluorophores near-to mixed metals as compared to either the virgin metals or from control samples containing no metals. Given the growing interest of MEF in the life sciences, then mixed metal substrates may well find utility over the individual metals, particularly in surface immunoassays where absolute brightness and photostability remain a primary concern.

2.0 Materials and methods

2.1 Materials

Toluene, fluorescein, Rose Bengal, *N*-acetyl-tryptophan-amide (NATA) and Phenylalanine (Phe) were purchased from Sigma. The concentration of NATA and Phe was determined by measuring the optical density of the solutions using extinction coefficients of $E_{280} = 5300$ M^{-1} cm^{-1} and $E_{257} = 195$ M^{-1} cm^{-1}, respectively.[24,25] Bovine serum albumin (BSA) was purchased from Sigma. To determine the concentration of the protein in

[a]Department of Biotechnology Engineering, Faculty of Engineering Science, Ben-Gurion University of the Negev, P.O. Box 653, Beer-Sheva, 84105, Israel
[b]Institute of Fluorescence and Department of Chemistry and Biochemistry, The Columbus Center, University of Maryland Baltimore County, 701 East Pratt Street, Baltimore, MD, 21202, USA. E-mail: geddes@umbc.edu
† Electronic supplementary information (ESI) available: Additional results are shown in Fig. S1–S11. See DOI: 10.1039/c0jm04311g

This journal is © The Royal Society of Chemistry 2011

J. Mater. Chem., 2011, **21**, 6179–6185 | 6179

solutions, an extinction coefficient of $E_{280} = 43\ 824$ M^{-1} cm^{-1} was used. Aluminium wire, 99% pure, for thermal vapor deposition onto glass slides was purchased from the Kurt J. Lesker Company, Material Group (Clairton, PA). Chromophores, including amino acids and protein, BSA were dissolved in TE buffer, pH 7.4.

2.2 Measurements of absorption and fluorescence

Absorption spectra of the fluorophores, protein intrinsic chromophores and BSA were measured using a Varian Spectrophotometer in quartz B7 1 cm path-length cuvettes.

Fluorescence spectra of the fluorophores and BSA were recorded using a Cary Eclipse spectrofluorimeter (Varian, Inc., USA) at room temperature. The solutions were sandwiched between a quartz slide and a glass slide with deposited metal(s) (silver, aluminium and their mixture) and for the control sample, containing no metal, between quartz/glass slides.

2.3 Time-resolved fluorescence decay measurements

The fluorescence intensity decay functions of the fluorescein chromophore on metal slides of different compositions and thicknesses, and on glass (MEF control sample) were measured using a TemPro Fluorescence Lifetime System (Horiba Jobin Yvon, USA). The reference cell contained colloidal silica, SM-30 ludox solution, used as a control (zero lifetime). Measurements were performed at room temperature. Determination of fluorescein excited state lifetimes (τ_i) and corresponding amplitudes (α_i) was undertaken using the TemPro Fluorescence Lifetime System software, DAS 6.

The emission intensity decays were analyzed in terms of the multiexponential model:

$$l(t) = \sum_i \alpha_i \exp(-t/\tau_i) \qquad (1)$$

where α_i are the amplitudes, the sum of which equals to 1.0, and τ_i are the decay times. The fractional contribution of each component to the steady-state intensity can be given as:

$$f_i = \frac{\alpha_i \tau_i}{\sum_j \alpha_j \tau_j} \qquad (2)$$

The mean lifetime of the chromophore excited state was calculated using the following equation:

$$\bar{\tau} = \sum_i f_i \tau_i \qquad (3)$$

The amplitude weighted fluorescence lifetime was calculated as follows:

$$\langle \tau \rangle = \sum_{i=1}^{n} \alpha_i \tau_i, \qquad (4)$$

where n is the number of fluorescence decay components in the total decay function. The values of the amplitudes and decay times were determined using nonlinear least-squares impulse reconvolution with a goodness-of-fit χ^2 criterion.

2.4 Numerical FDTD simulations

The 2D computational simulations of the electric field intensities and near-field distributions around metal nanoparticles were undertaken for three systems: (a) two 250 nm silver nanoparticles separated by 40 nm free space; (b) 30 nm aluminium nanoparticle (NP) and (c) their mixture—30 nm aluminium NP is centered between two 250 nm silver NPs, separated by 40 nm, using the Finite Difference Time Domain (FDTD) method. TFSF (total field scattered field) sources are used to divide the computation area or volume into total field (incident plus scattered field) and scattered field only regions. The incident p-polarized electric field was defined as a plane wave with a wave-vector that is normal to the injection surface. Using FDTD Solution software (Lumerical, Inc., http://www.lumerical.com), the simulation region was set to 700×450 nm^2 with a mesh accuracy of 5. To minimize simulation times and maximize resolution of field enhancement regions around the particle arrangement, a mesh override region is set to 1 nm around the nanoparticles. The overall simulation time was set to 50 fs and calculated over a broad wavelength range, using known permittivity values and refractive indices of silver and aluminium. The wavelength dependence of the NPs extinction, and cross-sections of its components, absorption and scattering were calculated using Lumerical software script. To simulate effects of water polarity on plasmon resonance spectra, the background index was set to the corresponding refractive index of water, 1.333.

2.5 Preparation of silver-island films (SiFs)

Silver-island films were prepared according to the procedure found in ref. 3. Deviations in SiF thickness were reduced by using a selection of silane-prep™ slides. The slides were stored in a vacuum between SiFs preparations to reduce possible oxidation.

2.6 Thermal vapor deposition of aluminium

Deposition of aluminium onto glass slides and on silver coated slides (SiFs) was performed using an AUTO 306 Vacuum Coater instrument, equipped with the quartz crystal sensor and SQM-160 Rate/Thickness Monitor (BOC Edwards, USA) for measuring. Thickness of the deposited aluminium on glass slides and on slides coated with silver nanoparticles (SiFs) ranged from 2 to 16 nm, as measured using the quartz-crystal sensor system. Real-color photographs of the aluminium and mixed (aluminium + silver) slides, used in this study, are shown in Fig. 1S†.

2.7 Atomic force microscopy (AFM)

AFM images were obtained on a molecular imaging PicoPlus microscope. Samples were imaged at a scan rate of 1 Hz with a 512×512 pixel resolution in a tapping mode.

3.0 Results and discussion

To study the effects of mixed-metal substrates (MMS) on enhanced fluorescence intensities, we have thermally evaporated aluminium onto glass substrates containing preformed

silver-island films (SiFs), where individually both SiFs and aluminium slides also served as control samples. As a function of aluminium deposition, the slides are seen to become increasingly optically dense as evidenced by the photographs in Fig. 1 and Fig. 2S–6S†. AFM images for 2 nm aluminium deposits on glass, Fig. 2S†, show surfaces comprised of small "rice like" nanoparticles, more evident in the phase contrast image of Fig. 1 and Fig. 2S† right. As the thickness of the aluminium is increased, Fig. 2S–6S†, the surface appears much more continuous. In contrast, AFM images of SiFs deposits on glass show much bigger island deposits, consistent with recent reports, Fig. 1.[26] However, when 2 nm aluminium is deposited on the SiFs, we see the "rice like" structures effectively coating the SiFs, Fig. 1, the phase contrast images, showing the aluminium nanostructured texture over the SiFs. The horizontal line scan of Fig. 3Sb† also shows an increase in surface roughness between the SiFs and coated SiFs samples, cf., Fig. 3Sa right and 3Sb† right images. Similarly, Fig. 4S–6S† show aluminium deposits on SiFs for 8, 12 and 16 nm of aluminium respectively.

Absorption spectra of the samples, Fig. 2, show that both 2 and 8 nm aluminium coatings appear optically mirror like, with a somewhat flat absorbance until the deep UV, where the band at 250 nm is indicative of the plasmon absorbance of aluminium. The SiFs absorption spectra show the typical strong plasmon resonance bands from 380 to 500 nm,[26] which both broaden and increase in optical density for the thicker coatings of aluminium on the SiFs. This is consistent with the color photographs in Fig. 1S†, which also become less transparent for thicker aluminium coatings. To understand these colorimetric and optical density changes we have undertaken Finite Difference Time Domain (FDTD) Simulations, in essence numerical simulations to both explain and account for the experimental observations. Fig. 1b shows a region-of-interest (ROI) which has been selected from the AFM images of Fig. 1a. Interestingly, the enlarged ROI clearly shows the aluminium "rice like" deposits (Region y) on the SiFs (Region x).

We have subsequently approximated and modeled this condition using two silver nanoparticles and one aluminium nanoparticle centered between the SiFs, the sizes reflecting those approximated from the AFM images, Fig. 1c.
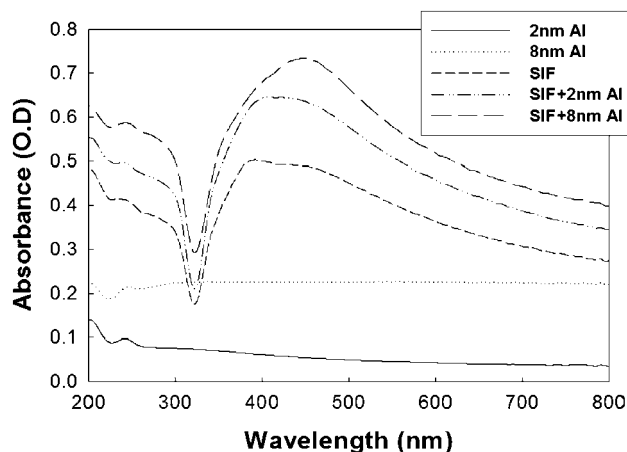

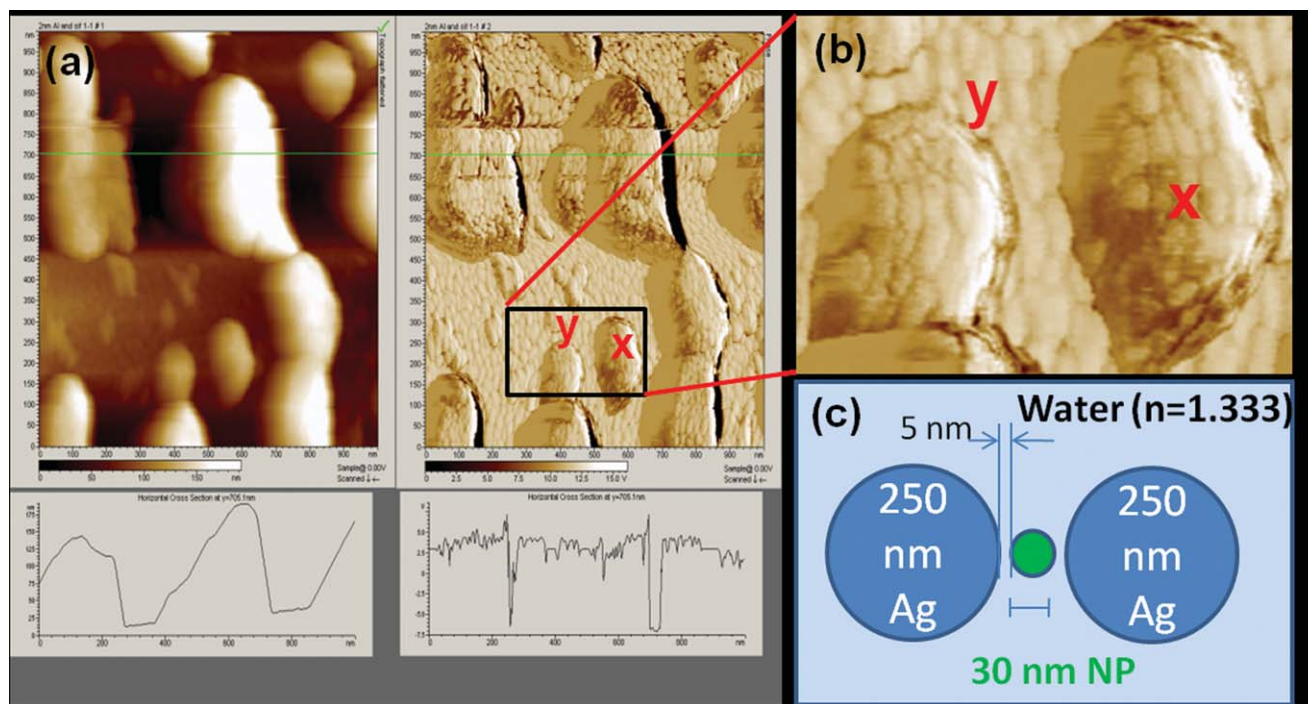**Fig. 2** Adsorption spectra of the different metalized slides shown in Fig. 1S†.

Fig. 1 (a) AFM images of 2 nm Al on SiFs (left), phase image (right). Below are the respective line scans for the AFM images. (b) Enlarged AFM phase image of 2 nm Al on SiF shown in black box in Fig. 1a, right. (c) Simplified model of Al–SiF geometry based on AFM measurements (see Fig. 1b). The model was used for the FDTD simulation of the E-field distribution around mixed metal nanoparticles.

Fig. 3 shows the respective theoretical electrical field simulations for the model. In the case of just two silver nanoparticles, Fig. 3c, we see a modest E-field intensity between the nanoparticles, considerably greater in magnitude than for the single aluminium particle shown in Fig. 3b. Fig. 3a shows the significantly enhanced electric field in the case of two silver nanoparticles and one centered aluminium nanoparticle. It is important to note the y-axis intensity scales for each respective image. The significant increases in electric field strength are further visualized when we consider the respective normalized plot of Fig. 3, *i.e.* Fig. 7S†. In this figure, one only sees an electric field in the top portion of the images, *i.e.* for the two silver and one aluminium nanoparticle construct.

In several recent papers Geddes and co-workers have postulated the mechanism underpinning MEF to be comprised of both an enhanced absorption (*i.e.* enhanced electric field effect) as well as an enhanced plasmon coupling component, the extent of MEF luminescence enhancement underpinned by the spectral overlap of a fluorophore's emission spectrum with the plasmon-scattering component of a nanoparticle's extinction spectrum.[16] This second mode of fluorescence enhancement has recently been experimentally verified,[16] and manifests itself by a shorter *system* luminescence/fluorescence lifetime, the surface plasmons in essence radiating the coupled quanta, in a system which is coupled in both the ground and the excited states.[16]

Subsequently to further understand the plasmon-coupling component in MEF mixed metal substrates, further simulations have been undertaken (Fig. 8S†). Fig. 8S† shows the extinction spectra (a), absorption (b) and scattering components (c) for the 3-particle model. Interestingly, all three spectra are typically broader for the 2 Ag and 1 Al nanoparticle system *i.e.* that considered in our ROI, Fig. 1b. Surprisingly, deconvolution of the respective spectra shows the presence of a new plasmon resonance band at ~540 nm, not present in the plasmon absorption spectra of the two individual metals themselves, Fig. 4. At this time we speculate that the new resonance band is due to the coupling and high-frequency dephased resonance of the surface plasmons from both metal types, not unlike the dephasing of similar resonances for identical metals, which have been shown to couple up to 2.5 times their diameter.[6] Interestingly, the ROI AFM image of Fig. 1 clearly shows the same particles are within this geometrical coupling consideration. It is worth noting that our model considers particles which are spatially separated and we have not modeled in the case of the Al directly coated onto the SiFs, which is far more complex, both sample embodiments present in Fig. 1.

To test the utility of the mixed metal substrates for MEF, we have considered both traditional and intrinsic fluorescent chromophores. For a solution of fluorescein sandwiched between the mixed metal substrates and a blank slide, we see further enhanced luminescence signatures as compared to the MEF from the individual metals, Fig. 5. This finding can also be observed visually in the color photographs of Fig. 5b, upper panel and Fig. 9S†, and suggests that mixed-metal substrates are a much better choice for applications in MEF, as compared to the widely used silver substrates. A similar result as for fluorescein can be seen for Rose Bengal, Table 1.

As briefly mentioned earlier, MEF affords for both enhanced luminescence intensities and reduced fluorophore lifetimes.
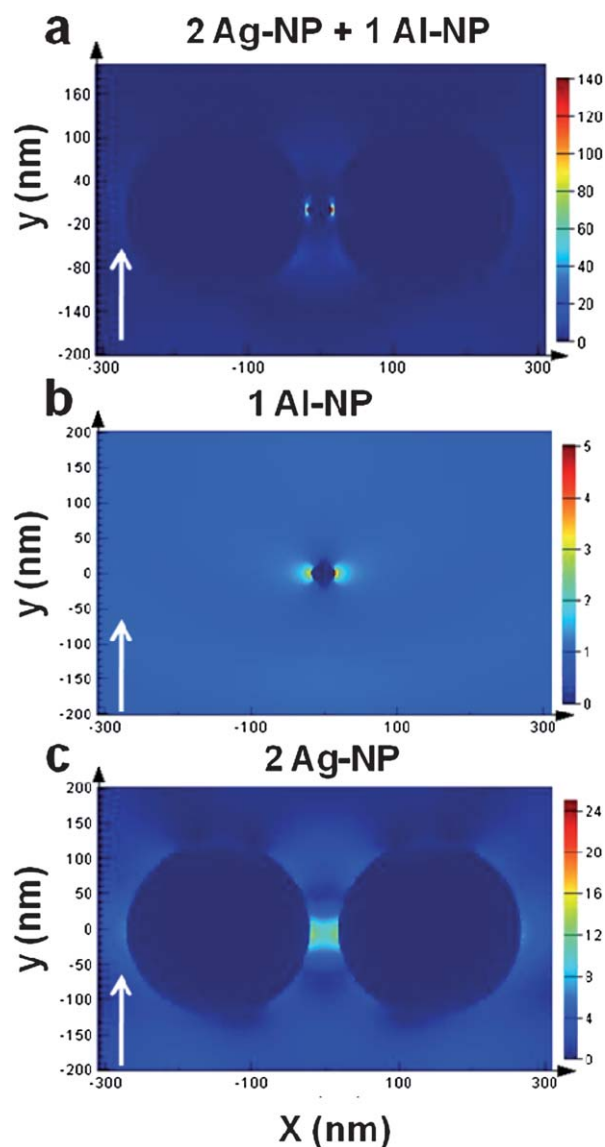

Fig. 3 Total E-field enhancement in the Al–Ag NPs system shown in Fig. 5. White arrows denote the injection axis in the FDTD simulations.

These observations are empirically underpinned by modifications to the classical far-field (greater than 1 wavelength of light away) rate equations. For a fluorophore in the far-field condition the free-space quantum yield, Q_0, is given by:

$$Q_0 = \frac{\Gamma}{\Gamma + k_{nr}} \tag{5}$$

and the fluorescence lifetimes by:

$$\tau_0 = \frac{1}{\Gamma + k_{nr}} \tag{6}$$

where Γ is the radiative rate, τ_0 is the free space lifetime and K_{nr} are the non-radiative rates.

In this free-space condition, any changes in a fluorophore's radiative rate invariably result in the quantum yield and lifetime, Q_0 and τ_0 respectively, changing in unison. However for MEF, Geddes has shown that these classical far-field considerations can be rewritten for the near-field condition,[3] such that:
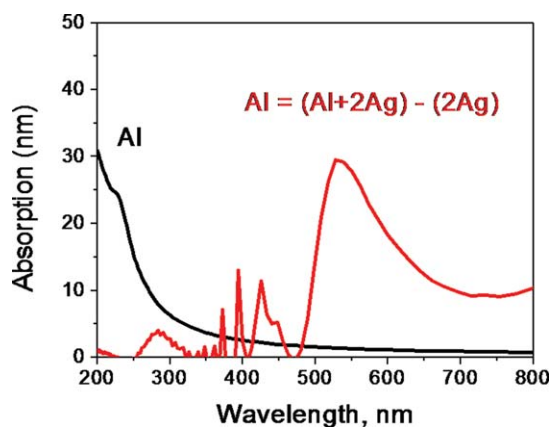
Fig. 4 Difference spectra (red) obtained by subtraction of absorption of two silver NPs (2Ag) from the absorption of two silver NPs + the aluminium NP (Al − 2Ag). Absorption spectra of aluminium NP (Al) are shown by black line. The size of Al-NP is 30 nm, Ag-NP is 250 nm (see Fig. 1c).

$$Q_m = \frac{\Gamma + \Gamma_m}{\Gamma + \Gamma_m + k_{nr}} \quad (7)$$

$$\tau_m = \frac{1}{\Gamma + \Gamma_m + k_{nr}} \quad (8)$$

where Q_m and τ_m are the metal modified quantum yields and lifetimes respectively.

To test whether mixed-metal substrates follow these near-field approximations, which have been shown to hold for numerous reports of single metals,[3,18] we have measured the time-resolved fluorescence decay times, Fig. 10S† and Table 2. Deconvolution analysis[5] of the decays in Fig. 10S† shows the greatest reduction in both amplitude weighted and mean lifetime, Table 2, consistent with the maximum fluorescein fluorescence enhancement shown in Table 1 and Fig. 5. This finding is completely consistent
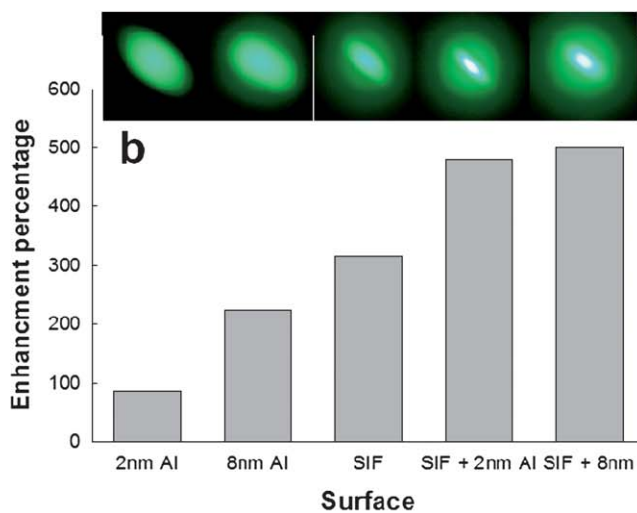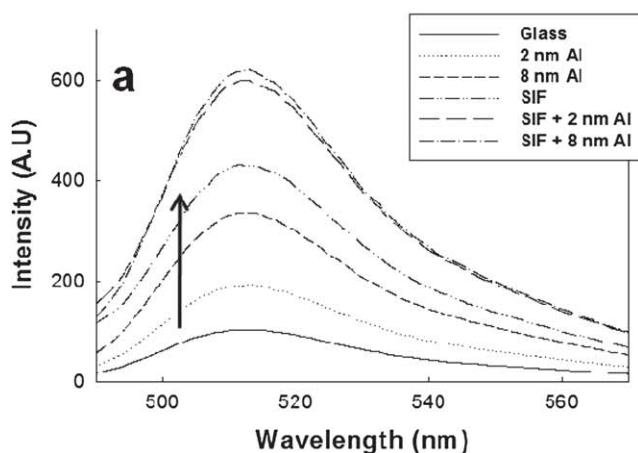
Table 1 Metal and mixed metal-based enhancement of fluorescence of the different chromophores in the UV and VIS spectral range[a]

Substrate	UV		VIS			
	Tn 285 nm	Phe 290 nm	BSA 330 nm	NATA 350 nm	Fl 520 nm	RB 565 nm
2 nm, Al	20	30	130	30	90	70
8 nm, Al	240	70	180	32	230	240
SiF	280	80	250	60	320	290
SiF + 2 nm Al	290	90	430	65	480	400
SiF + 8 nm Al	390	150	510	180	500	490

[a] Fl—sodium Fluorescein; Phe—Phenylalanine; NATA—N-acetyl-Tryptophan-amide; RB—Rose Bengal; Tn—Toluene. TE buffer, pH 7.6.

with current MEF thinking[4] and eqn (7) and (8). From eqn (7) and (8), we can readily see that an increase in the system radiative rate, Γ_m, provides for both an enhanced quantum yield, *i.e.* observed fluorescence intensity along with a reduced decay time (lifetime), consistent with our experimental observations.

It is well known that in classical far-field fluorescence spectroscopy, shorter fluorescence lifetimes are indicative of fluorophores with more enhanced photostabilities, due to these molecules spending less time in highly reactive excited states. Subsequently we have tested the mixed metal substrates using fluorescein. By measuring the steady-state intensity *vs.* time (*i.e.* photostability), one typically observes a greater photon flux from the mixed metal substrates, where the photon flux of the sample is proportional to the intergraded area under the respective curves (Fig. 11S†). When the samples are excitation adjusted to reflect the same initial steady-state emission intensity, we see a further significantly improved photostability from the mixed-metal substrates, as can be seen in Fig. 6. Given that absolute luminescence intensity and photostability are paramount in both microscopy[27] and fluorescence based assays,[6] then MMS offer

Fig. 5 (a) Fluorescein emission from the different metal depositions on glass slides. (b) Enhancement percentage of the different slides relative to a glass control sample containing no metal. Top panel: real color photographs of fluorescein emission from the different metallic surfaces, corresponding to the graph below (Fig. 5b). Excitation was at 473 nm (laser line) and emission was collected through a long pass filter.

This journal is © The Royal Society of Chemistry 2011

J. Mater. Chem., 2011, **21**, 6179–6185 | 6183

Table 2 Time resolved decay parameters of sodium fluorescein loaded on the different metal substrates[a]

Sample	τ_1/ns	τ_2/ns	α_1	α_2	τ/ns	$\langle\tau\rangle$/ns	χ^2
2 nm Al	5.09	2.74	0.81	0.11	4.42	4.93	0.939
8 nm Al	4.42	2.23	0.95	0.05	4.31	4.36	1.180
SiF	4.46	3.13	0.65	0.34	3.96	4.11	1.082
SiF + 2 nm Al	4.42	2.39	0.97	0.03	4.36	4.39	1.275
SiF + 8 nm Al	4.43	2.62	0.89	0.11	4.23	4.30	1.098

[a] The concentration of fluorescein in TE buffer, pH 7.6 was 10^{-4} µM. τ—mean lifetime, $\langle\tau\rangle$—the amplitude weighted lifetime.
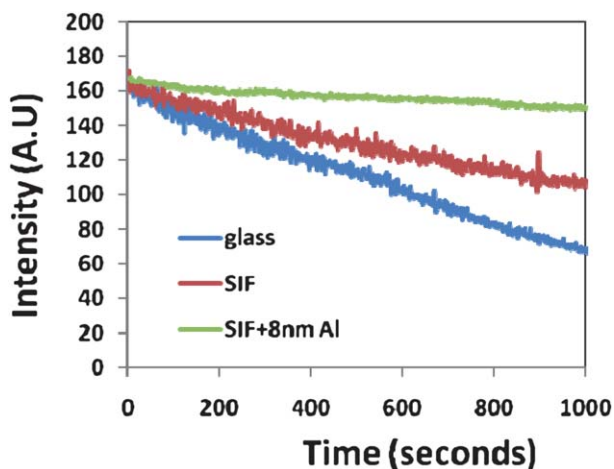

Fig. 6 Steady-state intensity decays of fluorescein emission from metal slides, SiF and SiF covered with aluminium (SiF + 8 nm Al), and glass slides. The initial intensity adjusted to give the same steady state intensity at time $t = 0$.

a potentially new solution to this well-recognized old problem. The utility of MMS in microscopy and indeed Fluorescence Correlation Spectroscopy (FCS) will be reported in due course.

3.1 Mixed-metal substrates (MMS) in the UV spectral region

Over the last few years there has been interest in the MEF literature in developing surfaces for MEF in the UV spectral region, particularly for the potential labeless detection of biomolecules, *i.e.* Metal-Enhanced Fluorescence of intrinsic protein residues, where metals such as aluminium and indium have been reported to date.[28,29] To test whether MMS would *also* enhance UV luminescence labels we have considered solutions of phenylalanine (Phe) and tryptophan (NATA), Fig. 7. Similar to the visible wavelength fluorophores fluorescein and Rose Bengal, mixed metal substrates (MMS) also provide for enhanced luminescence of these intrinsic protein residues. Interestingly, solutions of BSA (Bovine Serum Albumin) also show enhanced intrinsic protein luminescence, Fig. 7, with BSA known to contain 21 tyrosine and 3 tryptophan residues.[30] Further, our findings suggest that the UV enhancing properties of MMS are more pronounced as compared to the individual metals, as evidenced by the trends in Fig. 5 and 7 and Table 1, which could be an effect of the appearance of a new MMS plasmon absorption band, as shown in Fig. 4.

Finally, we have questioned whether the MMS could also enhance intrinsic solvent emission. Table 1 shows that toluene emission is also enhanced on the MMS, suggesting the potential use of MMS in applications such as scintillation counting,[31] where solvent emission detectability is a primary concern.

4.0 Conclusions

In this paper we have shown that mixed metal substrates made from both aluminium and silver nanodeposits can enhance luminescence very effectively over a broad wavelength range, enabling the enhanced luminescence from UV protein residues, solvents, as well as traditional visible wavelength fluorophores to be realized. This wavelength enhancing range is much broader than silver alone,[3] and indeed any individual metal surface reported in the MEF literature to date. In all fluorophore cases,
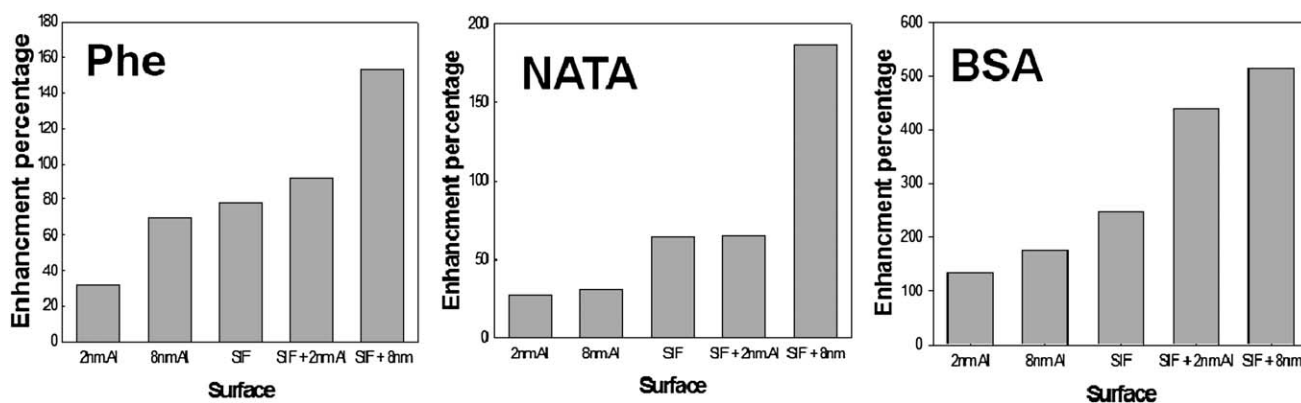

Fig. 7 Enhancement percentage from the different slides relative to a glass control sample containing no metal. Phe—phenylalanine; NATA—*N*-acetyl-tryptophan-amide; BSA—bovine serum albumin.

the enhancement trends are also very similar, suggesting the properties of the surfaces fundamentally underpin broad spectral enhancement. Our findings subsequently suggest that MMS are a much better choice over conventional single-metal substrates for applications in MEF. Transition from a single-metal surface to the mixed-metal NPs surface opens perspectives for the creation metal-coated films with broad spectral and enhanced MEF properties, which will have a great impact on the various biomedical assays utilizing fluorescence.

Acknowledgements

References

1 S. D'Agostino, P. P. Pompa, R. Chiuri, R. J. Phaneuf, D. G. Britti, R. Rinaldi, R. Cingolani and F. Della Sala, *Opt. Lett.*, 2009, **34**, 2381.
2 A. I. Dragan, E. S. Bishop, J. R. Casas-Finet, R. J. Strouse, M. A. Schenerman and C. D. Geddes, *Anal. Biochem.*, 2010, **396**, 8.
3 C. D. Geddes and J. R. Lakowicz, *J. Fluoresc.*, 2002, **12**, 121.
4 C. D. Geddes, *Metal-Enhanced Fluorescence*, John Willey & sons Inc., Hoboken, New Jersey, 2010.
5 J. R. Lakowicz, *Principles of Fluorescence Spectroscopy*, Springer Science + Business Media, LLC, New York, 2006.
6 K. Aslan, I. Gryczynski, J. Malicka, E. Matveeva, J. R. Lakowicz and C. D. Geddes, *Curr. Opin. Biotechnol.*, 2005, **16**, 55.
7 K. Aslan, M. J. R. Previte, Y. X. Zhang, T. Gallagher, L. Baillie and C. D. Geddes, *Anal. Chem.*, 2008, **80**, 4125.
8 S. Mackowski, S. Wormke, A. J. Maier, T. H. Brotosudarmo, H. Harutyunyan, A. Hartschuh, A. O. Govorov, H. Scheer and C. Brauchle, *Nano Lett.*, 2008, **8**, 558.
9 E. G. Matveeva, I. Gryczynski, A. Barnett, Z. Leonenko, J. R. Lakowicz and Z. Gryczynski, *Anal. Biochem.*, 2007, **363**, 239.
10 K. H. Drexhage, *J. Lumin.*, 1970, **1–2**, 693.
11 B. N. J. Persson, *J. Phys. C: Solid State Phys.*, 1978, **11**, 4251.
12 M. H. Chowdhury, K. Aslan, S. N. Malyn, J. R. Lakowicz and C. D. Geddes, *J. Fluoresc.*, 2006, **16**, 295.
13 Y. X. Zhang, K. Aslan, M. J. R. Previte, S. N. Malyn and C. D. Geddes, *J. Phys. Chem. B*, 2006, **110**, 25108.
14 Y. X. Zhang, K. Aslan, M. J. R. Previte and C. D. Geddes, *J. Fluoresc.*, 2007, **17**, 345.
15 Y. X. Zhang, K. Aslan, M. J. R. Previte and C. D. Geddes, *Appl. Phys. Lett.*, 2007, **91**, 023114.
16 Y. Zhang, A. Dragan and C. D. Geddes, *J. Phys. Chem. C*, 2009, **113**, 12095.
17 K. Aslan, S. N. Malyn and C. D. Geddes, *Chem. Phys. Lett.*, 2008, **453**, 222.
18 K. Ray, R. Badugu and J. R. Lakowicz, *Langmuir*, 2006, **22**, 8374.
19 K. Aslan and C. D. Geddes, in *Metal-Enhanced Fluorescence*, ed. C. D. Geddes, John Wiley & Sons Inc., Hoboken, New Jersey, 2010.
20 S. Chowdhury, V. R. Bhethanabotla and R. Sen, *Appl. Phys. Lett.*, 2009, **95**, 131115.
21 Y. Zhang, L. N. Mandeng, N. Bondre, A. Dragan and C. D. Geddes, *Langmuir*, 2010, **26**, 12371.
22 S. Lal, N. K. Grady, J. Kundu, C. S. Levin, J. B. Lassiter and N. J. Halas, *Chem. Soc. Rev.*, 2008, **37**, 898.
23 H. Wang, D. W. Brandl, P. Nordlander and N. J. Halas, *Acc. Chem. Res.*, 2007, **40**, 53.
24 E. A. Burstein, *Intrinsic protein luminesence. Model studies*, VINITI, Academy of Science, USSR, Moscow, 1977.
25 A. P. Demchenko, *Ultraviolet Spectroscopy of Proteins*, Springer-Verlag, New York, 1986.
26 R. Pribik, A. I. Dragan, Y. Zhang, C. Gaydos and C. D. Geddes, *Chem. Phys. Lett.*, 2009, **478**, 70.
27 T. G. Phan and A. Bullen, *Immunol. Cell Biol.*, 2010, **88**, 438.
28 M. H. Chowdhury, K. Ray, S. K. Gray, J. Pond and J. R. Lakowicz, *Anal. Chem.*, 2009, **81**, 1397.
29 A. I. Dragan and C. D. Geddes, *J. Appl. Phys.*, 2010, **108**, 094701.
30 K. Hirayama, S. Akashi, M. Furuya and K. Fukuhara, *Biochem. Biophys. Res. Commun.*, 1990, **173**, 639.
31 D. H. Wilkinson, *Applications of liquid scintillation counting*, North Holland, Amsterdam, 1974.